ADVANCES IN THE CONTROL OF A "SMART TUBE" HIGH POWER BACKWARD WAVE OSCILLATOR*

E. Schamiloglu,† G.T. Park, V.S. Soualian, C.T. Abdallah, and F. Hegeler
Department of Electrical and Computer Engineering
University of New Mexico, Albuquerque, NM, 87131, USA

Abstract

Previous accomplishments pertaining to the control of various parameters of an intense beam-driven relativistic backward wave oscillator (BWO) include maintaining a specified or desired output power over a determined frequency bandwidth, and maintaining a constant frequency over a wide range of power. This was accomplished using an iterative learning control (ILC) algorithm that yielded the appropriate input variables for the electron beam, as well as the appropriate displacement of the slow wave structure from the cutoff neck. A problem of much greater complexity is the simultaneous control of both frequency and power, involving the independent mapping of both power and frequency dependence on the two input variables: cathode voltage and slow wave structure displacement. The resultant two-variable system has been successfully implemented and tested for convergence with minimal iterations. In this paper we present an overview of our "smart tube," its development, and our most recent results.

I. INTRODUCTION

The notion of a "smart tube" high power microwave (HPM) source evolved from our earlier experiments studying the efficiency characteristics of a high power BWO driven by our Sinus-6 electron beam accelerator [1]. This device produces a 10 ns FWHM beam current pulse at voltages ranging from about 350-700 kV, and can operate at a pulse repetition rate as large as 200 Hz. (In practice, the accelerator operates at a pulse repetition rate no greater than 0.1 Hz, limited only by the capacitor bank used to energize the magnetic field-producing solenoidal coil.) The conclusion of our earliest research suggested that a slow wave structure (SWS) with an axially nonuniform coupling impedance can yield enhanced beam-to-microwave power conversion efficiency.

As part of this study we noticed a very strong dependence of the output power and frequency of the device on the exact axial position of the SWS with respect to the cutoff neck inlet to the electrodynamic structure. This dependence on axial position (*viz.* the dependence on

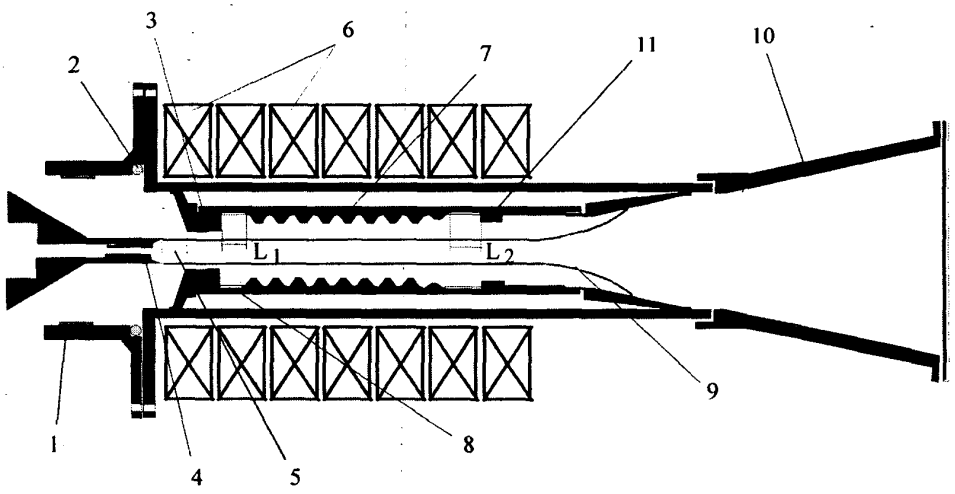

Figure 1. Experimental setup for BWO experiments with forward and backward shifting (axial displacement of the slow wave structure). Shown in the diagram are (1) capacitive voltage divider, (2) Rogowski coil, (3) cutoff neck, (4) cathode, (5) A-K gap, (6) magnetic field coils, (7) slow wave structure, (8) smooth circular waveguide and shifting lengths L_1 and L_2, (9) electron beam, (10) output horn antenna, and (11) reflection ring (not used).

* This work is supported through a High Energy Microwave Devices Consortium funded by an AFOSR/DOD MURI grant and administered through Texas Tech University. The acquisition of laser, optical, and brazed ceramic vacuum components were funded by FY'96 and FY'97 AFOSR DURIP grants.

† edl@eece.unm.edu

0-7803-5498-2/99/$10.00@1999 IEEE.

axial displacement of the SWS) indicated as distance L_1 in Fig. 1. In our detailed experiments and particle-in-cell (PIC) code simulations [2] we demonstrated a periodic dependence of the radiated power and frequency from this BWO on the axial displacement of the SWS. It was this periodic dependence on the output characteristics of our HPM source that we exploited to achieve a "smart tube." A neural network model was developed to describe the input/output characteristics of our HPM source [3]. Furthermore, an ILC algorithm was developed to achieve the control objectives using a minimal number of iterations [4]. A computer-controlled, motorized vacuum SWS displacement mechanism was designed and constructed to implement the changes required to achieve the specific outputs predicted by the ILC algorithm. Since the experimental hardware, the principle of achieving frequency agility using the displacement of the SWS, and the neural network modeling and preliminary ILC algorithm have been discussed elsewhere [1-4], we proceed to present a discussion of the more recent ILC work, implementation, and its results in the remainder of this paper.

II. ITERATIVE LEARNING CONTROL

From a controls perspective, it turns out that the fast dynamics and changes in the operating characteristics of an intense beam-driven relativistic BWO render traditional automatic control methods ineffective. Previously suggested ideas on using expert systems in the control of microwave tubes will in fact be ineffective as one can not control the tube during the course of a single shot. Feedback control methods, even sophisticated ones (such as adaptive, intelligent, and expert) all need a finite time between measurement and control action. Iterative Learning Control (ILC) is the one method that proved useful in this context due to the repetitive nature of our experiment, and to the fact that control actions may be implemented between shots [4]. A static model is too fast to be controlled in real time while maintaining the same order dynamics (and thus the same bandwidth and speed of response) of the open-loop system. Since the University of New Mexico's (UNM's) Sinus-6 driven BWO is repetitively-pulsed, one can attempt to achieve the control objectives between pulses.

For the ILC algorithm, measurements of microwave power and frequency must be consistent from one shot to the next. The accuracy and efficiency of the algorithm depend on this, whereas the correlation between actual and indicated values is irrelevant. A block diagram of the ILC procedure is indicated in Fig. 2.

III. IMPLEMENTATION OF ILC

Beam current and cathode voltage are measured using a *Rogowski coil* and capacitive divider, respectively (Fig. 1). These diagnostics were calibrated by sending a 5 kV pulse back into the transmission line through the cathode connection. The known input pulse was then compared to the signals obtained experimentally. The efficiency of microwave generation can be obtained by comparing the product of the maximums of these measurements to peak microwave power. Microwave power is determined using a crystal diode detector downstream of in-line attenuation, a power splitter and several meters of RG-214/U cable. The detector itself is an open-ended section of WR-90 waveguide placed approximately 1.2 meters from the conical horn antenna. The area of the open-ended waveguide is 2.32 cm^2, with an effective aperture area ranging from 2.5-3.7 cm^2 over a bandwidth of 9-10 GHz. The conservative value of 3.7 cm^2 was used for calculations.

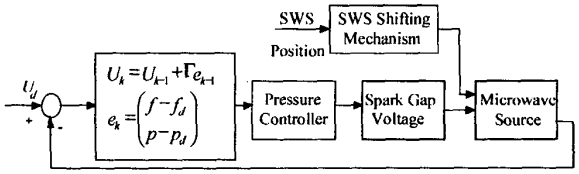

Figure 2. Block diagram of ILC procedure.

A major difference from previous experiments is the addition of a TM_{01} to TE_{11} mode converter placed between the beam dump and the horn antenna. Total power is thereby calculated by fitting the measured radiation pattern to a Gaussian distribution and performing a surface integral. For input to the ILC, however, the power density was used in order to minimize error introduced with the use of correction factors.

Periodic calibration of the microwave diagnostics is necessary because there is over 70 dB of attenuation between the crystal diode detector and the WR-90 antenna. Cables, attenuators, the power splitter and the crystal diode itself are calibrated using a network analyzer. The validity of the total power calculations was examined in previous experiments [5].

The frequency of the microwave signal is determined using the second branch of the split power signal. This signal is mixed with that of a Local Oscillator (LO), whose output is 9.0 GHz, and the resulting Intermediate Frequency (IF) is sent to an oscilloscope for capture. All signals are then directed to LabVIEW™ via a General Purpose Interface Bus (GPIB) for analysis and control input. The power signal is smoothed using a Butterworth filter before extracting an average of the maximum (95%) and peak values for control purposes. These steps were taken in order to reduce the instability caused by spikes and other anomalies. Frequency content is determined using a Fast Fourier Transform (FFT) on the IF signal. For the short pulse output of the Sinus-6 where virtually no mode-sharing or mode-jumping [6] occurs, this is generally sufficient.

In order to control the input parameters mentioned earlier, two devices were designed: 1) a motor-operated, vacuum-compatible SWS assembly for lateral shift (displacement) adjustments, and 2) a valve control system

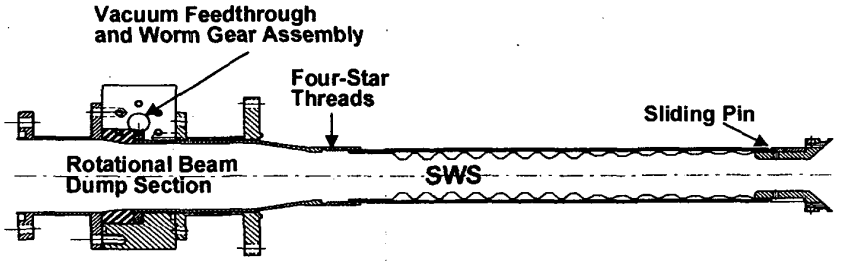

Figure 3. Vacuum slow wave structure displacement mechanism.

used to raise and lower nitrogen pressure in the spark gap switch. The SWS displacement utilizes a stepper motor to drive a worm-gear via a commercial, rotary motion, vacuum feedthrough (Fig. 3). The worm-gear actuates a screw mechanism which moves the entire SWS with respect to the anode and cutoff neck, allowing for the sinusoidal variation of frequency and power. Included with the assembly is a motor controller, which is operated either manually or through an RS-232 serial data link by LabVIEW™ at the host computer [7].

This assembly was designed with two major considerations. A sufficient range of motion for control purposes and the ability to reposition in ten seconds or less. Axial motion of the SWS is achieved through rotation of the four-start screw threads located on the rotating beam dump section, which is driven by the worm-gear. A conversion factor of 6,300 pulses/cm was obtained by taking into account the motor characteristics (pulses per revolution), worm-gear reduction factor, and thread pitch. As the motor turns clockwise or counterclockwise, the SWS will shift laterally a distance limited by the number of threads in the rotating beam dump section. This distance is approximately 2 cm.

It was determined experimentally that the range needed for control purposes is approximately eight millimeters; therefore, a distance of two centimeters meets the first condition. The latter constraint relates to the total charge time of the beam-focusing solenoid, which is the limiting factor for the repetition rate (0.1 Hz). Allowing for full range of motion within this time frame is highly desirable. To send instructions to the stepper motor controller, a subroutine was written in LabVIEW™. In general, the SWS is initialized to the zero millimeter position at the start of the run, then moved to the desired position according to the ILC algorithm. The second input variable is the cathode voltage, which may be adjusted by increasing or decreasing the nitrogen pressure in the spark gap. An on-off, nonlinear pressure control circuit with dead band and hysteresis was designed to control a set of valves used to charge or bleed nitrogen to and from the spark gap switch. The relationship between the nitrogen pressure and cathode voltage is nearly linear.

Currently, the cathode voltage control is not fully automated. The circuit uses a pressure transducer for actual pressure and compares it to a reference voltage set by the operator. The desired pressure, and therefore cathode voltage, is obtained by manually setting the reference voltage to a predetermined value (given by the ILC algorithm in the program).

In order to fully automate the control effort, a data acquisition card (DAQ) has been installed in the host computer. The reference voltage can be set here, or the entire valve circuit, with the exception of the solenoid valves, may be replaced by another subroutine. Changes to the input variables are determined by the ILC algorithm, which depends on the output parameters. The entire output range of operation was mapped with the aid of these components in order to model the frequency and power parameters with respect to the inputs.

IV. RESULTS AND CONCLUSIONS

Several data points were taken and averaged at each spark gap switch pressure and SWS displacement between 10-15 atm and 0-8 mm, respectively. Power and frequency were recorded and a second order planar fit in two variables was determined using MathCad™. Prior to using the control gain in the actual implementation, it was tested in a simulation program written in MathCad™. A desired power and frequency along with an acceptable error were entered as inputs, while the output consisted of the converging iterations. To increase the realism of the simulation and test the stability of the gain, a random number generator effectively added ±5 kV to the simulated input voltage on every pass. The results indicated a stable system, with the number of iterations depending on the allowable error. Increasing the randomly generated input voltage (simulating an errant shot) produced a predictably unstable system. Because shots like these occur on occasion, the actual subroutine was designed to disregard any shot that was not within ±15 kV of the predicted cathode voltage value.

We thus demonstrated simulation results that were stable for a combined power and frequency error < 0.5% and < 0.01% when the cathode voltage was within ±5 kV of the predicted value, and unstable for an error < 0.01% when the cathode voltage was within ±20 kV of the predicted value.

All that remained after achieving successful simulation results for the BWO model was to develop the ILC algorithm on the host computer. The cathode voltage was converted to spark gap pressure using a linear fit of the

data obtained on its performance, and then was converted to a low-voltage reference signal calibrated by a pressure transducer. Similarly, the lateral shift position of the SWS was converted to stepper motor pulses using the conversion factor described earlier.

Figure 4 shows the response of the ILC algorithm for desired power and frequency inputs of 200 kW/cm^2 and 9.7 GHz, respectively. Although the algorithm converged in two iterations, it was allowed to continue for demonstration purposes. The significance of this is that lower tolerances could have been achieved with a higher number of iterations.

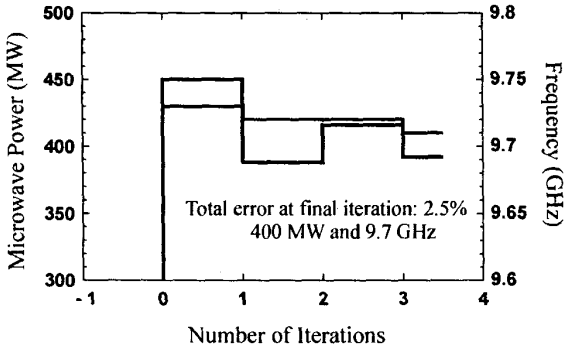

Figure 4. Response of ILC algorithm converging to specified performance.

In the next example (Fig. 5) we show how the ILC can never converge if the desired power and frequency values are outside the operating range. It is impossible for this device to produce an output power of 140 kW/cm^2 with a frequency of 9.58 GHz.

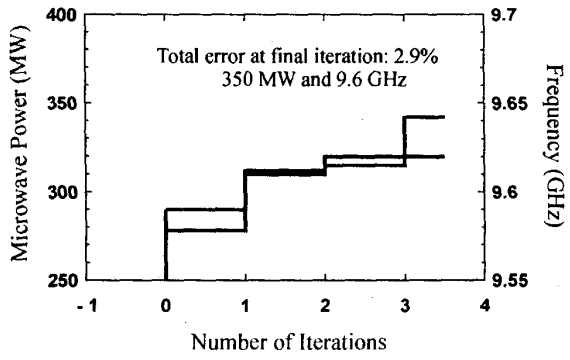

Figure 5. Response of ILC when performance objectives are not attainable.

Many other successful examples have been recorded. The conclusion is that the robust ILC algorithm usually converges in less than five iterations, as long as reasonable values for power, frequency and tolerance are chosen.

In conclusion, we have demonstrated the first performance of a gigawatt level "smart tube" HPM source. Future work includes the incorporation of an *in-situ*, remotely adjustable A-K gap as an additional input to add even enhanced control capabilities.

REFERENCES

[1] L.D. Moreland, E. Schamiloglu, R.W. Lemke, S.D. Korovin, V.V. Rostov, A.M. Roitman, K.J. Hendricks, and T.A. Spencer, "Efficiency Enhancement of High Power Vacuum BWOs Using Nonuniform Slow Wave Structures," IEEE Trans. Plasma Sci., vol. 22, 554, 1994.

[2] L.D. Moreland, E. Schamiloglu, R.W. Lemke, A.M. Roitman, S.D. Korovin, and V.V. Rostov, "Enhanced Frequency Agility of High Power Relativistic Backward Wave Oscillators," IEEE Trans. Plasma Sci., vol. 24, 852, 1996.

[3] C. Abdallah, W. Yang, E. Schamiloglu, and L.D. Moreland, "A Neural Network Model of the Input/Output Characteristics of a High Power Backward-Wave Oscillator," IEEE Trans. Plasma Sci., vol. 24, 879, 1996.

[4] C.T. Abdallah, V.S. Soualian, and E. Schamiloglu, "Towards Smart Tubes Using Iterative Learning Control," IEEE Trans. Plasma Sci., vol. 26, 905, 1998.

[5] E. Schamiloglu, R. Jordan, M.D. Haworth, L.D. Moreland, I.V. Pegel, and A.M. Roitman, "High Power Microwave-Induced TM_{01} Plasma Ring," IEEE Trans. Plasma Sci., vol. 24, 6, 1996.

[6] C. Grabowski, E. Schamiloglu, C.T. Abdallah, and F. Hegeler, "Observation of the Cross-Excitation Instability in a Relativistic Backward Wave Oscillator," Phys. Plasmas, vol. 5, 3490, 1998.

[7] Designed and constructed by Garron Instruments, Elkay, Oregon (Dr. Gary Rondeau, President).